

Interaction and Cooperative Nucleation of InAsSbP Quantum Dots and Pits on InAs(100) Substrate

Karen M. Gambaryan

Received: 19 November 2009 / Accepted: 9 December 2009 / Published online: 24 December 2009
© The Author(s) 2009. This article is published with open access at Springerlink.com

Abstract An example of InAsSbP quaternary quantum dots (QDs), pits and dots–pits cooperative structures' growth on InAs(100) substrates by liquid phase epitaxy (LPE) is reported. The interaction and surface morphology of the dots–pits combinations are investigated by the high-resolution scanning electron microscope. Bimodal growth mechanism for the both QDs and pits nucleation is observed. Cooperative structures consist of the QDs banded by pits, as well as the “large” pits banded by the quantum wires are detected. The composition of the islands and the pits edges is found to be quaternary, enriched by antimony and phosphorus, respectively. This repartition is caused by dissociation of the wetting layer, followed by migration (surface diffusion) of the Sb and P atoms in opposite directions. The “small” QDs average density ranges from 0.8 to $2 \times 10^9 \text{ cm}^{-2}$, with heights and widths dimensions from 2 to 20 nm and 5 to 45 nm, respectively. The average density of the “small” pits is equal to $(6\text{--}10) \times 10^9 \text{ cm}^{-2}$ with dimensions of 5–40 nm in width and depth. Lifshits–Slezov-like distribution for the amount and surface density of both “small” QDs and pits versus their average diameter is experimentally detected. A displacement of the absorption edge toward the long wavelength region and enlargement toward the short wavelength region is detected by the Fourier transform infrared spectrometry.

Keywords Quantum dots · Pits · Liquid phase epitaxy · Strain-induced · III–V compound semiconductors

Introduction

In the last two decades, a large research effort has been devoted to quantum dots (QDs), the quantum wires, QD chains, nanoholes and pits [1–8] due to their modified density of states, fascinating optoelectronic properties and device applications for lasers, photodetectors and other electronic devices. Among quantum dots, pits and wires fabrication techniques, the self-organized Stranski–Krastanow method [9] is an important one by which dislocation-free dots, elongated islands and wires can be produced. Indeed, above a certain critical thickness, the growth mode switches from the conventional layer-by-layer (i.e., two-dimensional, 2D) to a 3D growth mode due to the accumulation of the elastic energy in the strained layer that, first, partially relaxes by spontaneously nucleating small islands of strained material and, later, by creating misfit dislocations. The elastic strain caused by lattice mismatch can also be relaxed by the formation of undulations, pits and their combination [5–8]. Depending on the growth conditions, the elastic strain can be relaxed by the formation of either quantum wires and quantum dots, or even unique island–pit pairs. Extensive experimental results suggest that surface morphologies are relying on growth conditions and matrix materials. On the basis of an atomistic model, it is shown that the energy change due to the step formation is negative or positive depending upon the sign of the misfit. The step formation energy can even be negative for compressive misfit stress in the heterolayer, while it is definitely positive for tensile misfit stress. This conclusion is in contrast to the classical model where the step energy is always positive and independent of the sign of the misfit. The step formation energy influences the critical thickness and the energy barrier for dislocation nucleation.

K. M. Gambaryan (✉)
Department of Physics of Semiconductors and Microelectronics,
Yerevan State University, 1 A. Manoukian Str., Yerevan 0025,
Armenia
e-mail: kgambaryan@ysu.am

Using a simple atomistic simulation, it is shown that the critical thickness depends upon the sign of the misfit. For example, it changes from 4 nm for Ge films on Si(100) substrates to 6 nm for Si films on Ge(100) substrates having the same misfit [5]. The investigations of the surface morphology evolution of strained InAs/GaAs films at different growth conditions [6] demonstrated that there are at least three different strain relaxation mechanisms for the same material system. That is, depending on the growth conditions, the elastic strain can be relaxed by the formation of either quantum wires or quantum dots, or even unique island–pit pairs. The islands and pits first grow simultaneously as the layer deposition proceeds. Both the island height and the pit depth can be much greater than the average layer thickness. This suggests that considerable mass transport from substrate into the islands is taking place during the growth [7]. However, during heteroepitaxy, when the layer becomes sufficiently thick, the pits are eventually filled up either by the lateral overgrowth or by the expanding islands, forming nearly pure island morphology at the surface. The detailed analysis of the surface dynamics during phase transitions of GaAs(100) [10] and unusual role of the substrate at droplet-induced GaAs/AlGaAs QD pairs growth [11] also confirm this assumption.

From the industrial point of view, the narrow band gap III–V semiconductor materials like InAs, GaSb, InSb and their ternary and quaternary alloys are particularly interesting and useful since they are potentially promising to access mid-infrared and far infrared wavelength regions. These materials would provide the next generation of LEDs, lasers and photodiodes for applications such as infrared gas sensors, for molecular spectroscopy, thermal imaging, photovoltaic (PV) [12] and thermo-photovoltaic cells (TPV) [13]. The application of the InAsSbP and other similar quaternary materials opens up interesting physical and technological prospects for the dirigible growth of QDs, the pits and dots–pits cooperative systems. Independent variations of the third and fourth components provide corresponding sign of the misfit; i.e., providing the tensile or compressive misfit stress. At the first case, elastic strain will be relaxed by the formation of QDs, but at the second one—by the pits.

In this article, an example of InAsSbP quaternary QDs, the pits and dots–pits cooperative structure growth on InAs(100) substrates by LPE, as well as the interaction and surface morphology of the dots–pits combinations are presented and investigated.

Experimental Results and Discussion

The samples are grown by LPE using a slide-boat crucible. To ensure a high purity of the epitaxial layers, the entire growth process is performed under the pure hydrogen

atmosphere. The InAs(100) substrates have a 11 mm diameter are undoped, with a background electron concentration of $n = 2 \times 10^{16} \text{ cm}^{-3}$. The InAs_{0.742}Sb_{0.08}P_{0.178} quaternary alloy used here as basis composite is conveniently lattice-matched to InAs. The LPE growth solution components—undoped InAs, undoped InP and Sb (6 N) are solved in a In (7 N) solution that has been first homogenized for 1 h at $T = 580 \text{ }^\circ\text{C}$ and then 3 h at the initial growth temperature of $T = 550 \text{ }^\circ\text{C}$ to equilibrate the system thermodynamically. To expect the strain-induced QDs and pits formation, the undoped and supersaturated by antimony and phosphorus liquid phase was used to provide a different sign of lattice mismatch up to 4% between the InAs substrate and InAsSbP epilayer. To initiate the growth of QDs and pits, an oversaturation of the liquid phase is developed by decreasing the initial growth temperature up to 2 °C at the slower ramp rate.

The high-resolution scanning electron microscope (SEM-EDXA—FEI Nova 600—Dual Beam) is used to study the strain-induced InAsSbP QDs–pits cooperative structures. Bimodal growth mechanism for the both the QDs and the pits nucleation is observed. Interestingly enough (see Fig. 1) that the pits (large and small) like the islands primarily formed into truncated “reverse” pyramids. The EDXA measurements shown that, at first, either islands or pits edges have a quaternary composition and that on average, they are enriched by antimony and by phosphorus, respectively. In our InAsSbP quaternary experimental system, the nucleation mechanism of QDs and the exposure of wetting layer (and InAs substrate) at pits are quite interesting, but very complicated for explanation result. From a physical perspective, we have assumed that simultaneous nucleation of the islands and pits are occurring due to variable curvature (the tensile or compressive local perturbations) of the wetting layer. We suggest that at the perturbed sites, the wetting layer surface is strained, and the depositing material will prefer not to remain at these sites, but rather diffuse away. After that occurs, the strain relaxation is performed at the adatoms (Sb and P) surface diffusion in opposite directions, leaving behind the islands and the pits on the surface. In this scenario, corners or edges of the pits and islands are the most preferred sites to attach newly deposited materials, because at these regions, the strain energy is most relieved. The islands (or pits) at these relaxed regions will grow rapidly at the expense of the material around the pits (or dots). The fact that the “large” pits are deeper (up to 100 nm and more) than the wetting layer thickness implies that the arsenic atoms are also “pumped” out from the substrate and probably replaced by the phosphorus atoms. The similar cooperative nucleation of the dots–pits pairs was detected at the growth of InAs QDs on GaAs substrate [7], GaAs/AlGaAs QD pairs [11] and at the growth of In_{0.53}Ga_{0.47}As layers on InP(001) substrate [14, 15]. The effect of island density on pit nucleation in

$\text{In}_{0.27}\text{Ga}_{0.73}\text{As}$ films grown on GaAs(001) substrate is discussed in [16].

In order to be confident, we calculated the Gibbs free energy of InAsSbP quaternary alloy, as well as separately of InAs-InSb, InAs-InP and InSb-InP ternary alloys. We found that at $T = 550\text{ }^\circ\text{C}$ (our growth temperature), the Gibbs energy has the minimal value at $x = 0.39$ for $\text{InAs}_{1-x}\text{Sb}_x$ and at $y = 0.52$ for $\text{InAs}_{1-y}\text{P}_y$ alloys. Therefore, there is a trend for these binary pairs to mix. Otherwise, for the $\text{InSb}_{1-z}\text{P}_z$ ternary alloy at the same temperature, the sufficiently wide immiscibility gap is exist at $0.05 < z < 0.97$. In this concentration range, the Gibbs energy increases (from the both sides) and the mixing of these binary compounds becomes energetically not preferable. This result marginally proves our assumption that at the nucleation of InAsSbP quaternary dots and pits, the surface diffusion of the antimony and phosphorus in opposite direction has to be energetically more preferable. In addition, note that with the increasing of the liquid phase

initial concentration, the islands and pits shape transformation from the truncated pyramids to ellipsoidal and globe shape was detected.

Figure 2a displays the SEM and AFM images of the InAsSbP unencapsulated dots–pits cooperative structure in plain view for the surface area of $S = 4\text{ }\mu\text{m}^2$. In this figure, white points correspond to the QDs and black points to pits. The QDs and pits are clearly visible and quite uniformly distributed over the substrate surface. Figures 1b, c and 2b–d show that cooperative nucleation of the dots–pits structures is occurring. In particularly, the “large” pits are banded by quantum wires and that the QDs are banded by pits (in the form of “nano-camomile”).

Our statistical explorations show that the “small” QDs average density ranges from 0.8 to $2 \times 10^9\text{ cm}^{-2}$, with heights and widths dimensions from 2 to 20 nm and 5 to 45 nm , respectively. The average density of the “small” pits is equal to $(6\text{--}10) \times 10^9\text{ cm}^{-2}$ with dimensions of $5\text{--}40\text{ nm}$ in width and depth. Surface density of the “large”

Fig. 1 High-resolution SEM images of the InAsSbP strain-induced “large” pits banded by the quantum wires

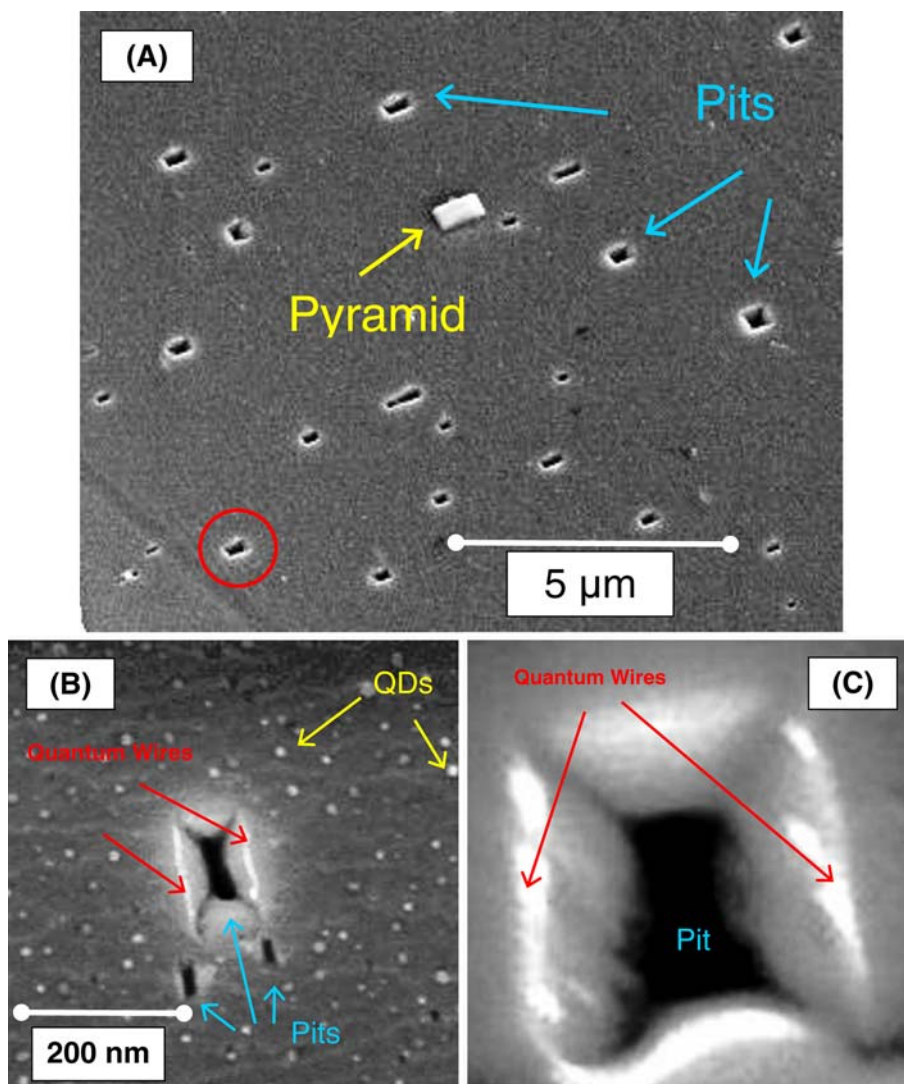
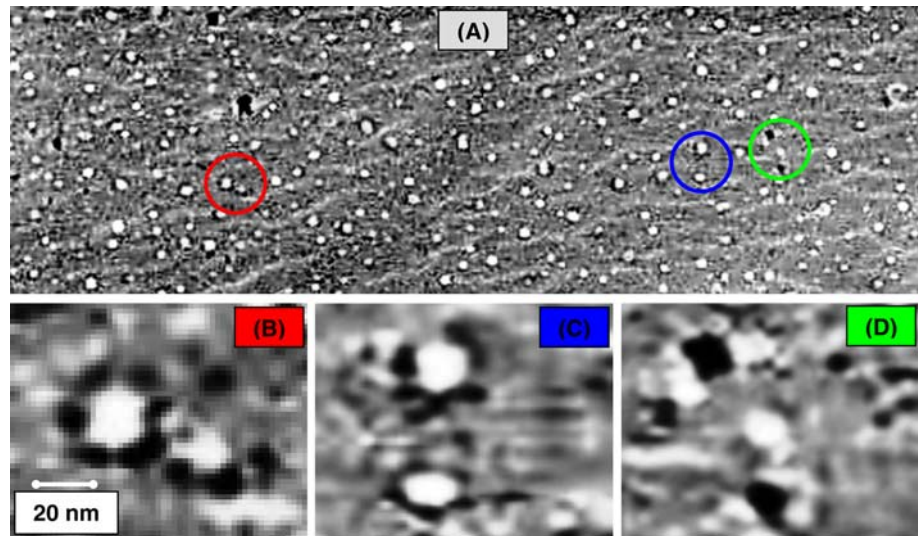


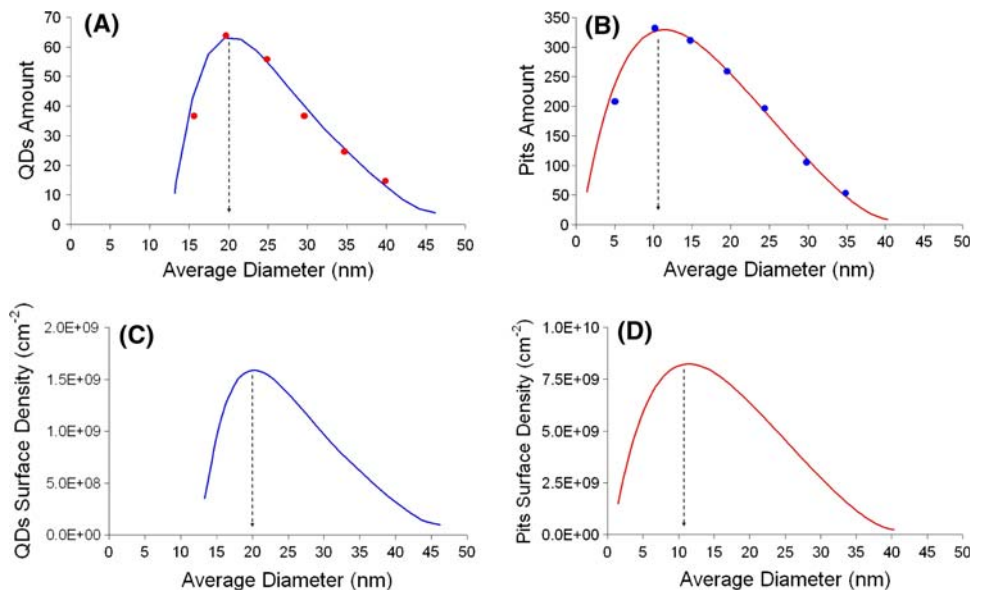
Fig. 2 High-resolution SEM images of the InAsSbP strain-induced QDs–pits cooperative structure—(a) ($S = 4 \mu\text{m}^2$). **b, c** and **d**—enlarged view of the mentioned by red, blue and green ovals related regions. White ovals—QDs, black ovals—pits



dots and pits is less by almost on two orders of magnitude. The Lifshits–Slezov-like [17] distribution for both “small” QDs and pit amount, and surface density versus their average diameter calculated from the surface of $S = 4 \mu\text{m}^2$ is detected and displayed in Fig. 3.

We used the Fourier transform infrared spectrometry (FTIR–Nicolet/NEXUS) to investigate the transmission spectra (see Fig. 4) of an unencapsulated InAsSbP dots–pits cooperative structure at room temperature. As a test sample, we used the same industrial InAs(100) substrate without QDs and pits. The result shows the displacement of the absorption edge toward the long wavelength region from $\lambda = 3.44 \mu\text{m}$ (for test sample) to $\lambda = 3.85 \mu\text{m}$, as well as the enlargement of the absorption spectrum up to $\lambda = 2.75 \mu\text{m}$ short wavelength region. We assume that this effect is the result of the absorption by the QDs through the permitted energy sub-band.

Fig. 3 Dependence of the InAsSbP strain-induced QDs and pits amount (a, b) and surface density (c, d) versus their average diameter ($S = 4 \mu\text{m}^2$). Legend keys—experimental data, curves—Lifshits–Slezov approximations



Schematic diagram showing the type II InAsSbP/InAs QDs is presented in Fig. 5. Energy levels’ assignments based on FTIR measurements and calculations by Eq. 1.

$$E_n = \frac{\pi^2 \hbar^2 n^2}{2m^* R^2} \quad (1)$$

where \hbar is the Planck constant, m^* is the light holes effective mass, R is the average diameter of QDs and n is the integer. The similar approach was applied in [18]. For our experimental system (at light holes confinements), $E_1 = 3.8 \text{ meV}$ (at $R = 50 \text{ nm}$), $\Delta E_{\text{max}} = 38 \text{ meV}$ (at $R = 16 \text{ nm}$), sub-band depth $U_0 \approx 42 \text{ meV}$ ($\approx 1.7 kT$), $m^* = 0.0384 m_0$. Numerical value for the light holes’ effective mass for our $\text{InAs}_{1-x-y}\text{Sb}_x\text{P}_y$ quaternary system was calculated by the linear approximation of the corresponding values for binary compounds at $x = 0.04$ and $y = 0.08$.

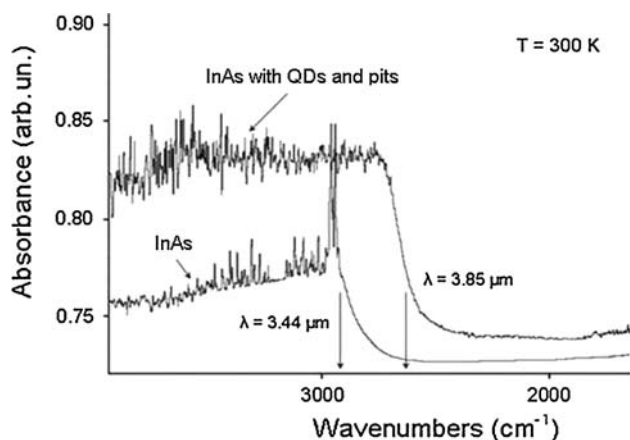


Fig. 4 Room temperature FTIR spectra of the InAs test sample and the InAsSbP QDs–pits cooperative structure grown on InAs(100) substrate

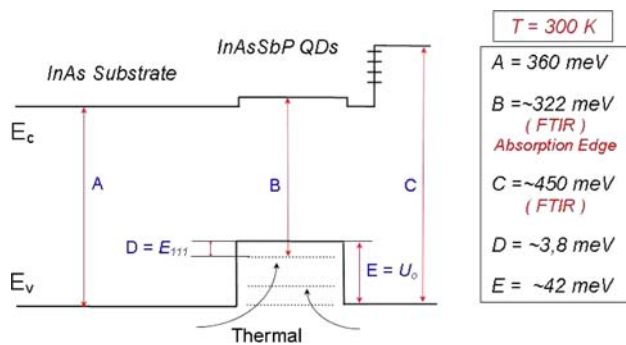


Fig. 5 Schematic view of the zone diagram showing the type II InAsSbP/InAs QDs–pits cooperative structure. Numerical values for B, C, D and E energies are approximate and based on FTIR measurements and calculations

Finally, note that at the growth of diode heterostructures with the quantum dots and pits inside p–n junction spatial charge region, the main challenge to overcome is providing the lateral overgrowth of the pits (providing “reverse” QDs) and keeping the dots size during epitaxy of the cap epilayer. We assume that by using step-cooling LPE, the growth of the cap epilayer from the strongly cooled liquid phase will address this problem.

Conclusion

Thus, we have presented an example of the InAsSbP quaternary QDs, pits and dots–pits cooperative structures growth on the InAs(100) substrates by LPE. The interaction and surface morphology of the dots–pits combinations were investigated. Bimodal growth mechanism for the both QDs and pits nucleation was observed. Lifshits–Slezov-like distribution for the amount and surface density of “small” QDs, and pits versus their average diameter was

experimentally detected. Application of the InAsSbP and other similar quaternary materials opens up interesting physical and technological prospects for the dirigible growth of QDs, pits and dots–pits cooperative systems. By the corresponding and independent variations of the V-group elements concentrations, the preferred nucleation of the dots or pits can be selected. The results of our study can be also used for producing controlled arrays of strain-induced QDs, which is very important for the fabrication of wide-band photodiodes, thermo-photovoltaic cells and other InAs-based mid-infrared devices.

Acknowledgments The author gratefully acknowledges Prof. V. M. Aroutiounian, Prof. P. Soukiassian, Prof. R. Fornari and Dr. T. Boeck for comprehensive support and fruitful discussions and Ms. M. Schulze (present location—“Bosch AG”) for SEM and AFM measurements. This work was carried out in the frame of Armenian National Governmental Program for Nano-Electronics and ISTC Grant A—1232.

Open Access This article is distributed under the terms of the Creative Commons Attribution Noncommercial License which permits any noncommercial use, distribution, and reproduction in any medium, provided the original author(s) and source are credited.

References

1. K. Nishi, H. Saito, S. Sugou, J.S. Lee, *Appl. Phys. Lett.* **74**, 1111 (1999)
2. D. Haft, R.J. Warburton, K. Karrai, S. Huan, G. Medeiros-Ribeiro, J.M. Garcia, W. Schoenfeld, P.M. Petroff, *Appl. Phys. Lett.* **78**, 2946 (2001)
3. K.M. Gambaryan, V.M. Aroutiounian, T. Boeck, M. Schulze, P.G. Soukiassian, *J. Phys. D Appl. Phys.* **41**, 162004 (2008)
4. Z.M. Wang, K. Holmes, Y.I. Mazur, G.J. Salamo, *Appl. Phys. Lett.* **84**, 1931 (2004)
5. M. Ichimura, J. Narayan, *Mater. Sci. Eng.* **B31**, 299 (1995)
6. Z. Gong, Z. Fang, Z. Miao, Z. Niu, *Int. J. Nanosci* **5**, 883 (2006)
7. J.H. Li, S.C. Moss, B.S. Han, Z.H. Mai, *J. Appl. Phys.* **89**, 3700 (2001)
8. Z.M. Wang, B.L. Liang, K.A. Sablon, G.J. Salamo, *Appl. Phys. Lett.* **90**, 113120 (2007)
9. I. Stranski, L. Krastanow, *Math.-Naturwissenschaft* **146**, 797 (1938)
10. Z.M. Wang, G.J. Salamo, *Phys. Rev. B* **67**, 125324 (2003)
11. Z.M. Wang, Y.I. Mazur, K.A. Sablon, T.D. Mishima, M.B. Johnson, G.J. Salamo, *Physica Status Solidi (RRL)* **2**, 281 (2008)
12. V.M. Aroutiounian, S.G. Petrosian, A. Khachatryan, K. Touryan, *J. Appl. Phys.* **89**, 2268 (2001)
13. V.A. Gevorkyan, V.M. Aroutiounian, K.M. Gambaryan, A.H. Arakelyan, I.A. Andreev, L.V. Golubev, Yu.P. Yakovlev, *Solid State Electron.* **52**, 339 (2007)
14. A.J.Y. Lee, C. Pearson, J.M. Millunchick, *J. Appl. Phys.* **103**, 104309 (2008)
15. A. Riposan, C. Pearson, J.M. Millunchick, *Appl. Phys. Lett.* **90**, 091902 (2007)
16. A. Riposan, G.K.M. Martin, M. Bouville, M.L. Falk, J.M. Millunchick, *Surf. Sci.* **525**, 222 (2003)
17. I.M. Lifshits, V.V. Slezov, *J. Phys. Chem. Solids* **19**, 35 (1961)
18. S.-S. Li, J.-B. Xia, Z.L. Yuan, Z.Y. Xu, W. Ge, X.R. Wang, Y. Wang, J. Wang, L.L. Chang, *Phys. Rev. B* **54**, 11575 (1996)